Geometric strategies to design a bistable deployable structure with straight scissors using stiff and flexible rods

Corresponding Author	
Full name	Carlos José García Mora
Name in scientific papers	Carlos J. García - Mora
Affiliation	Architecture School of Seville University, Spain (PhD candidate) Department of Building Structures and Geotechnical Engineering
Phone	+34 671 93 25 15
E-mail address	email@carlosjosegarciamora.com

Co-author	
Full name	Jose Sánchez Sánchez
Name in scientific papers	Jose Sánchez - Sánchez
Affiliation	Architecture School of Seville University, Spain (Professor) Department of Building Structures and Geotechnical Engineering

Abstract

For many years, the design of bistable deployable structures with straight scissors has been focused on evaluating the structural behaviour of rods during the deployment according to the application of loads. These structures have recently begun to be built with some rods composed of a flexible material in order to concentrate the deformations in these rods. The techniques that are currently used to design and calculate these structures require an assumption of the application of loads. In this article, two novel strategies for the design of this type of structures are proposed. The first is based on the study in situ of the structure's deployment process and the second combines the knowledge that currently exists about the change of geometry during the deployment with FEM.

Keywords: Geometry; Deployable structure; Scissor; **Mechanism**; Folding; Kinematics; Flexible rod; **Stiff** rod; Straight rod

1. Introduction

The world of deployable structures can be basically divided into two big groups: structures of rods [1] [2] and structures of surfaces [3] [4]. On the one hand, the first group is composed of straight scissors (polar or translational units) [5] [6] [7], bended scissors (angulated units) [8] [9] or foldable rods structures [10] [11] [12] [13]. On the other hand, the second group is represented by Origami [14] [15] [16] and Kirigami [17].

With this in mind, the research of this paper will be focused on deployable structures of straight scissors. This transformable system is a **mechanism** with joints and rods and where the whole transformation between its two limit positions (folded and unfolded) can be reached using an input force [18] [19] [20] (Figure 1).

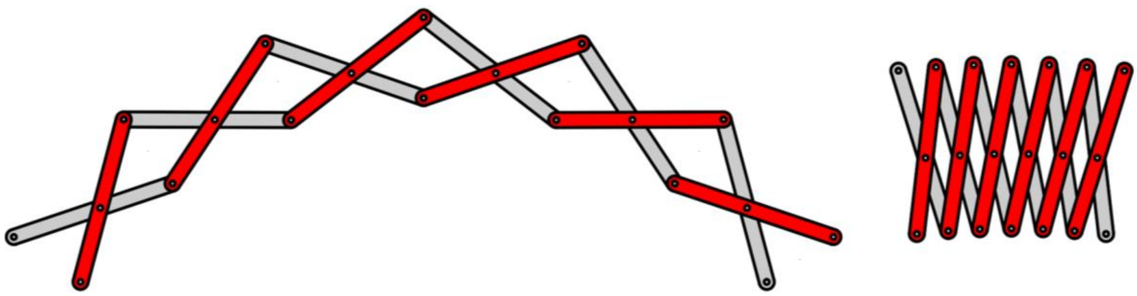

Fig. 1. Example of a deployable structure with polar units.

A simple way to classify this type of structures is based on the energy accumulated in the rods during the deployment process [21]. If there are not geometric incompatibilities during the deployment process and the only elastic deformations in the structure is due to the weight of the elements, the structure is a **mechanism**.

However, if there are variations in the length of the rods due to geometric incompatibilities during the deployment process and these variations disappear in the folded and unfolded position, the structure is called “bistable” [22] [23] [24] [25] [26]. Its practical use has been quite limited due to the huge complexity which they present in terms of calculation and optimisation, and its design can only be applied to isolated modules and simple geometries. Despite this fact, these structures have multiple advantages such as the stability of the geometry in the final position of the deployment, a greater capacity to absorb loads (in comparison with a **mechanism**) and a better definition of the geometry [27] [28] [29].

An example of this situation can be observed in Figure 2 a) and Figure 2 b), where some loads have been applied to a deployable and bistable structure with a spherical shape (these loads reproduce the external forces during the deployment process). Finally, the deformations and stresses in the rods for the most unfavourable case are represented in Figure 2 c).

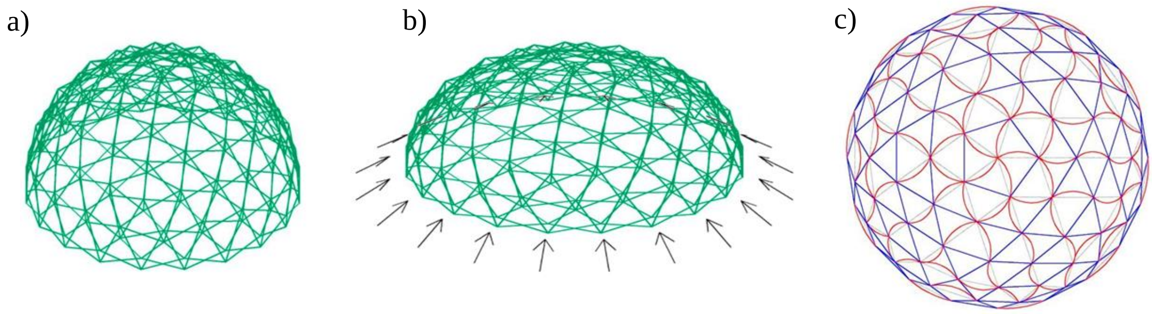

Fig. 2. a) Bistable deployable structure with spherical shape b) Middle phase during the deployment due to the application of forces c) Deformation of the rods during the deployment (red rods = compression and blue rods = traction).

Currently, the calculation problems of these structures have been solved due to the development of specialised algorithms and the obtaining of deformations and maximum stresses during the deployment process are more straight forward (Figure 3).

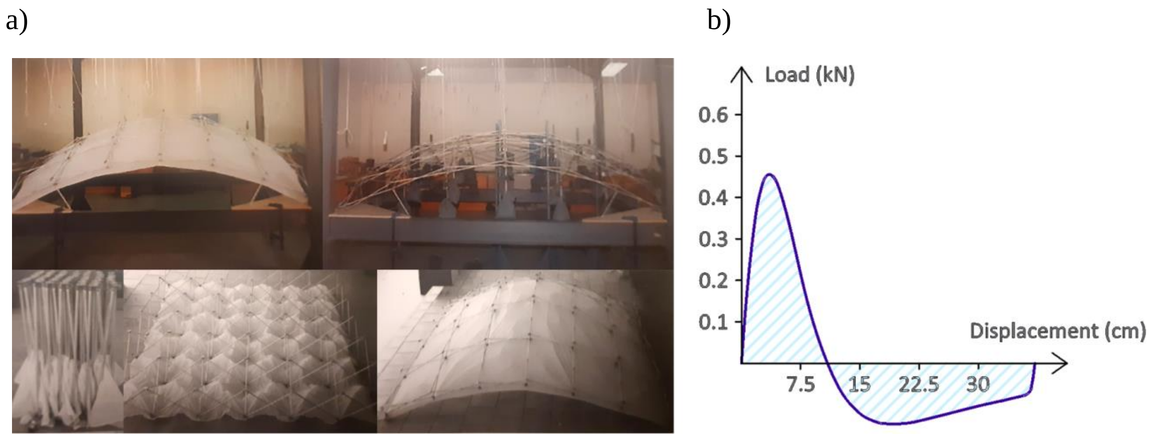

Fig. 3. a) Bistable sphere designed and built by the authors of this paper b) Load-displacement curve of the bistable sphere on the right against a gradual load.

All the rods were **stiff** in Figure 2 and Figure 3 and, consequently, there was no preference in the distribution of the deformations. To solve this situation, bistable deployable structures have begun to be designed with a combination of flexible rods and **stiff** rods. The goal is to obtain a low deformation in **stiff** rods during the deployment process because the deformations are going to be concentrated in flexible rods. **In this context, the concept "stiff rods" is referred to the rods that will have a low deformation during the deployment process due to the bistability phenomenon. On the other hand, the concept "flexible rods" is referred to the rods that will absorb the deformations during the deployment process due to the bistability phenomenon.**

Consequently, 2 geometric methods will be developed for the design of deployable structures with **stiff**-flexible scissors and the results obtained from the geometric simulation will be compared with the results from FEM and from the built models. Finally, a deployable structure at human scale using the second method of this research will be calculated in function of the Eurocode regulation for structures.

2. Methods

2.1. Method 1: Method based on the deployment process

2.1.1. Development of the method

The first proposed method consists in the use of the modules of Figure 4 a) or Figure 4 b), depending on the deployment process (red rods = flexible rods and black rods = **stiff** rods). This explanation will be developed taking as example the design of a bistable sphere:

- Step 0: The designer starts from a deployable element whose behaviour during the deployment is predictable; for example, a triangular module, a square module, a ring, etc. (Figure 4 c).

- Step 1: Triangular modules that belong to the design geometry and composed of **stiff** rods are obtained from the external faces of the step 0 module (Figure 4 d). This distribution of rods will be closed with the module of Figure 4 a) or of Figure 4 b). (The blue points are the connecting joints with the previous part of the structure). **To know the correct one, a simulation of the deployment process shall be done in a CAD software. This simulation has been performed using a combination of Rhinoceros and Grasshopper 3D where the trajectory was predicted using a parametric algorithm. Since the system works as a mechanism, there is only one degree of freedom and, consequently, the positions of all points can be obtained for each stage**

of the deployment. If the green points move away, the structure will be closed with Figure 4 a) and, if they move close, the structure will be closed with Figure 4 b). In this case they move away so Figure 4 a) will be used and the result is Figure 4 e).

- Step 2: The process of step 1 is repeated. In this case, the vertices of two consecutive triangles move close, which causes a movement away from the next pair of triangles. Consequently, one pair of triangles is going to be closer and another pair of triangles is going to be further away, so both modules of Figure 4 a) and Figure 4 b) will be used (Figure 4 f). Finally, the same process will be repeated until the surface is completely designed (Figure 4 g).

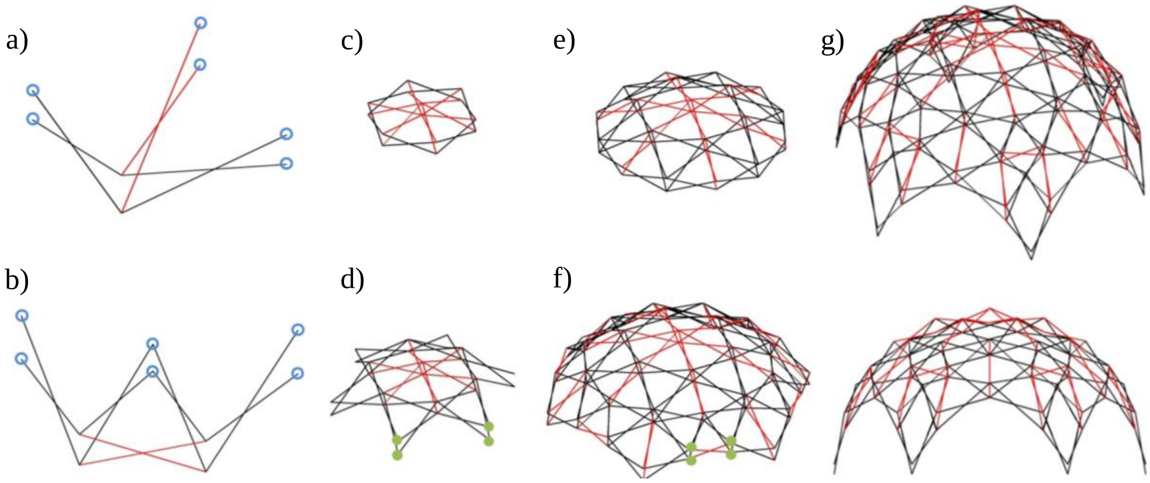

Fig. 4. a) Module type 1; b) Module type 2; c) Initial deployable element; d) Triangles growing from the step 0; e) End of step 1 using module type 1; f) End of step 2 using module type 1 and 2; g) Perspective and front view of the final bistable structure.

Likewise, the use of this method guarantees that the deformations in the **stiff** rods during the deployment process and due to the geometric incompatibilities are very low because these deformations are going to be concentrated in the flexible rods.

This situation is checked using SAP200 where curved finite elements and a linear analysis have been used (Second order effects are not considered and the joints are represented as points) (Figure 5). The calculation model represented in the following picture will be used in the whole research.

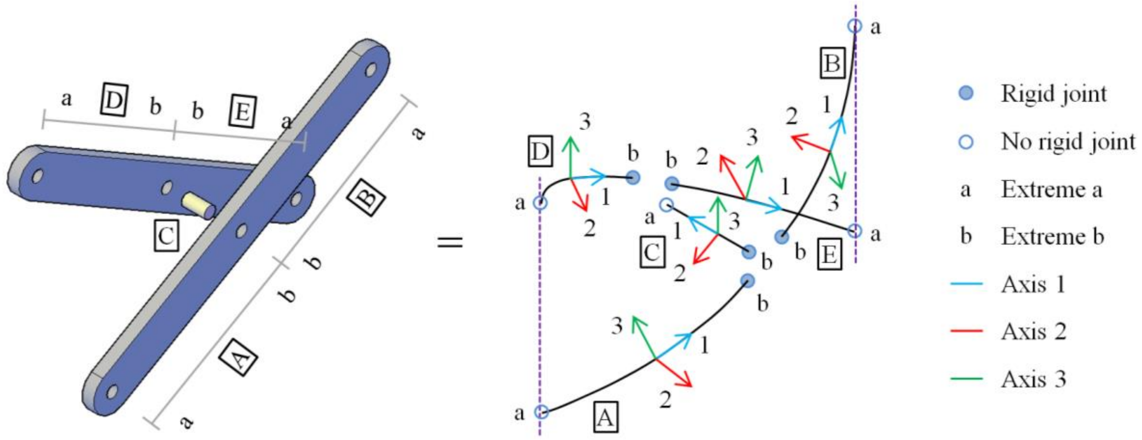

Fig. 5. Calculation model of a scissor in Sap2000.

The boundary conditions are:

a) Length of rod C ≈ 0

b) Moment of rod C in "a" (Axis 2 and 3) = 0

c) Moment of rod C in "a" (Axis 1) ≠ 0

d) Moment of rod A,B,D,E in "a" (Axis 1,2 and 3) ≠ 0

Likewise, different stages of the deployment process are represented in Figure 6 (black rod = **stiff** rod and red rod= flexible rod).

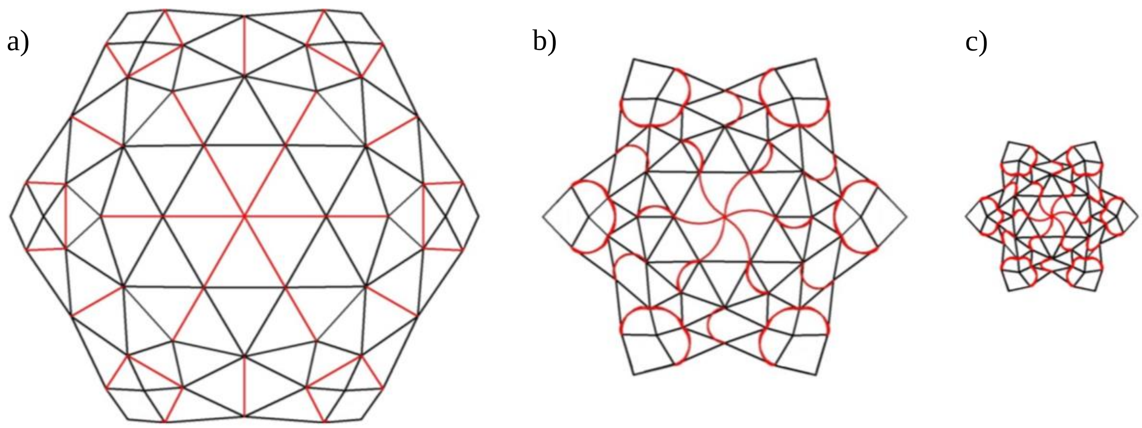

Fig. 6. a) Floor view of the sphere of Figure 4 in the deployed position b) 66% of the deployment process c) 33% of the deployment process.

It is important to highlight that if a full deployment of the structure is required, the design of the previous triangular tessellation can only be achieved using the convergence surface method [30] [31] [32] with the intersection of a family of convergence ellipsoids [33] [34]. If 4-sided polygonal modules are used, the methods of Niels de Temmerman and Kelvin Roovers can also be applied [35] [36].

2.1.2. Built model

To prove this method, a model of the previous sphere has been built (Figure 7). The material of **stiff** rods is DM (Thickness=3 mm, width=5mm, E=4000 N/mm^2 and ρ=730 kg/m^3) [37] [38] [39] and the material of flexible rods is ABS (Thickness=1.5 mm, width=5mm, E=1100 N/mm^2 and ρ=650 kg/m^3) [40] [41]. The joints have been done with a flexible tube that allows the required rotations.

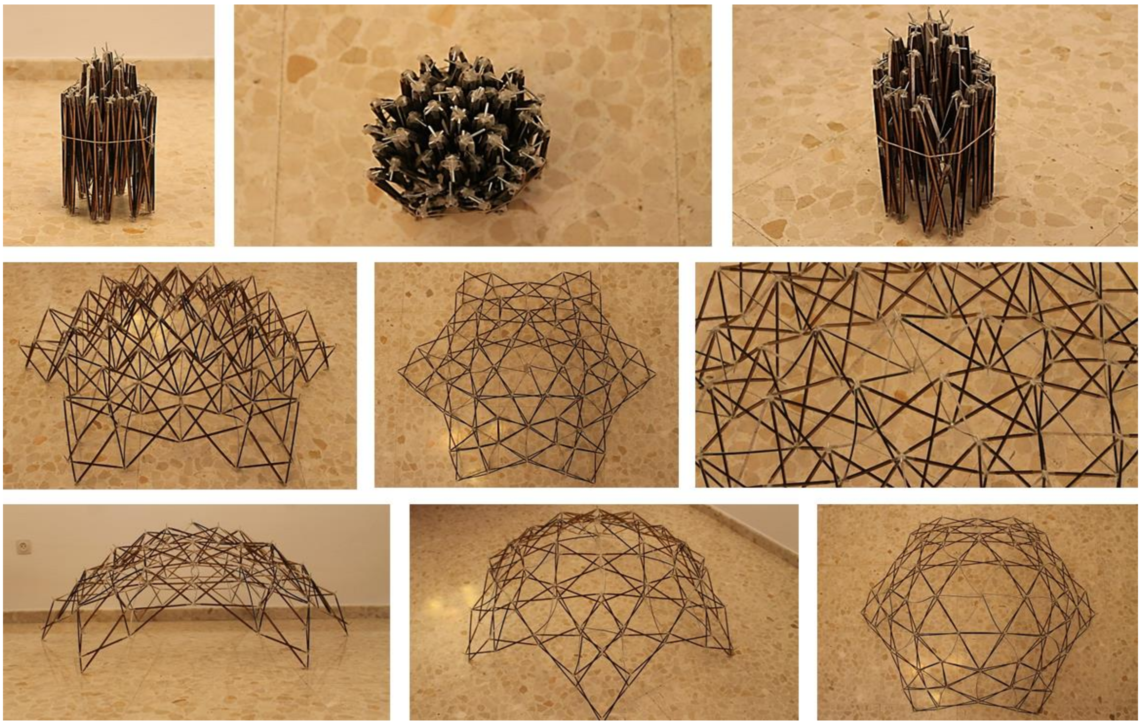

Fig. 7. First row: Folded position; Second row: Position where flexible rods have the highest deformation; Third row: Deployed position with a diameter of 1.25 m.

In addition, details of the joints used in this physical model are represented in the following picture (Figure 8), where each rod will have a plastic tube connected in each extreme and the connection between the scissors is achieved using a screw that joins the plastic tubes together (diameter of the screws = 2.5mm). This constructive solution not only provides all necessary angles of rotation in the space but also it introduces a small eccentricity in the structure with a simple assembly procedure.

a) b)

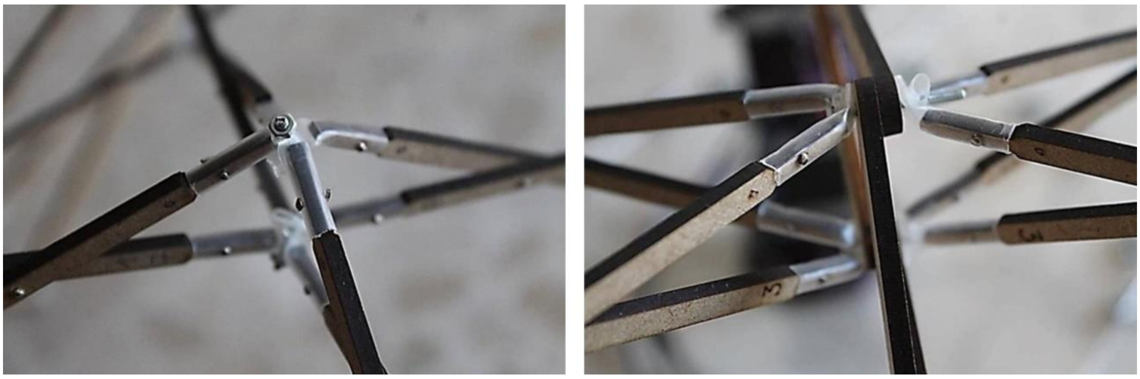

Fig. 8. a) Joint for a general case of scissors b) Joint that connects a plane of scissors with other scissors coming from different angles in the space (not used in the physical models of this research).

2.1.3. Results

Finally, the deformations of each scissor are compared between the geometric simulation (Grasshopper software), the FEM simulation and the measurements of the model (Figure 9). From this comparison, it is important to highlight that:

- Geometric simulation: This analysis will be developed assuming that the **stiff** rods have not any deformation due to the geometric incompatibilities during the deployment process. Consequently, all deformations will be absorbed by the flexible rods.
- FEM simulation: The eccentricity of the joints is not considered (joints are simulated as points) and the forces have been applied in the joints B with a vertical direction. The forces during the deployment process of the built model will be applied in the same joints with the same direction.
- Built model: Flexible joints will be used in order to allow all rotation angles in the space.

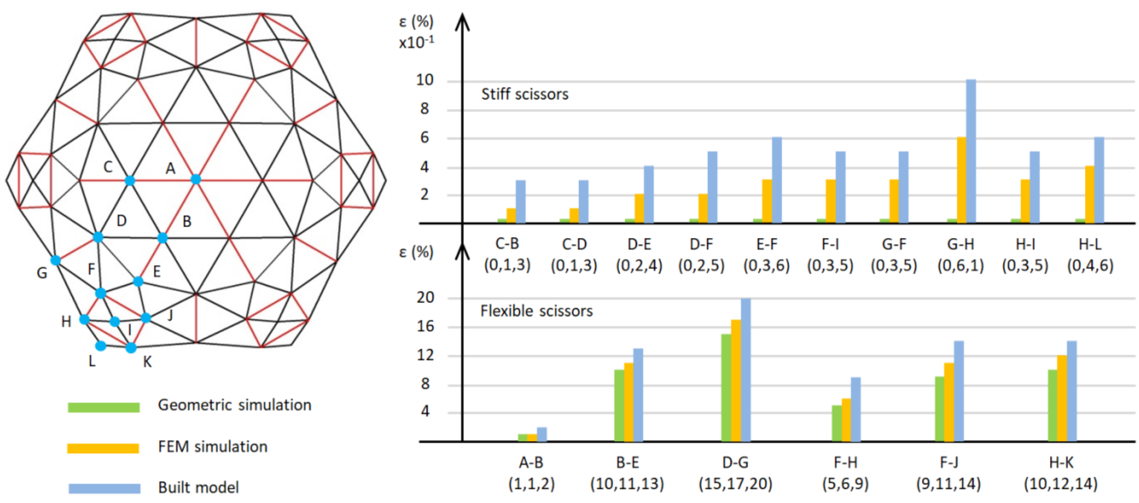

Fig. 9. Comparative graph of the highest deformations in the scissors. Values on **stiff** scissors are x10-1.

The following considerations shall be highlighted from the Figure 9:

- The null value of the deformations in the geometric simulation for the **stiff** scissors is due to the assumption that all deformations from the geometric incompatibilities during the deployment are concentrated in the flexible rods. This assumption allows the measurement of the deformations in the flexible scissors because the **stiff** scissors will have the behaviour of a mechanism with only one degree of freedom.
- The difference of the deformations between the FEM simulation and the built model for the **stiff** scissors and for the flexible scissors is due to the simplification of the joints in the FEM simulation. The connections between the rods have been developed using a flexible material that allows all rotation angles. However, these joints have also an important influence in the structure due to the lack of stiffness.
- The difference of the deformation between the FEM simulation and the geometric simulation for the flexible scissors is due to the no consideration of the weight of the elements in the geometric simulation.

2.1.4. Dimension of the rods (the middle joint will be in the centre of each rod)

Stiff rods (units in cm)					
	C-B	**C-D**	**D-E**	**D-F**	**E-F**
Rod 1	27.10396	31.23742	24.23658	28.59780	22.96430
Rod 2	27.10396	25.98205	24.48231	22.74918	16.86984
	F-I	**G-F**	**G-H**	**H-I**	**H-L**
Rod 1	16.64932	26.57041	26.66378	16.74198	31.78150
Rod 2	13.01449	22.05260	34.09140	25.05293	20.35458

Flexible rods (units in cm)						
	A-B	**B-E**	**D-G**	**F-H**	**F-J**	**H-K**
Rod 1	28.65605	25.35823	33.93626	33.26990	21.23744	23.28277
Rod 2	26.34228	20.34853	23.56973	21.32411	21.23744	23.28277

Table 1. Length of all rods (spherical physical model).

2.2. Method 2: RiBiCo method (Rigidisation – Bistability – Cover)

2.2.1. Physical principles

Although the previous method provides satisfactory results, the design of the deployable structure needs a considerable time and effort since it is necessary to simulate the deployment process of each module. To deal with this situation, another faster, more systematic and general method has been developed with the following principles:

a) Principle 1: Suppose 2 elastic solids with different module of elasticity that share a displacement condition and where a distributed load is applied (the own weight is not considered). For a very small E ratio value (E = Elasticity module), the solid with the highest E will behave as a rigid solid (solid without deformation). If this situation is extrapolated to a bistable deployable structure, a high difference between the elastic modules of the stiff scissors and the flexible scissors means that the stiff scissors will have a low deformation and the flexible scissors will absorb almost all deformations during the deployment process.

b) Principle 2: It is known that deployable structures lose its curvature quickly during the deployment process (Figure 10).

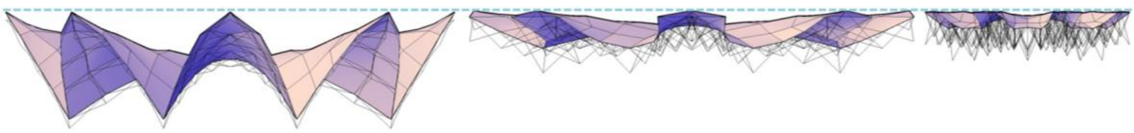

Fig. 10. Fast loss of curvature during the deployment process in a double curvature geometry.

To reproduce this behaviour, a distributed load is applied to the external shape of the deployable structure (this load could be its own weight) and the flexible scissors will be in the directions of the stresses of compression.

2.2.2. Development of the method

Once the principles of the method have been established, the next step is to develop the stages. To make this process more visual, the method is going to be applied to 3 different geometries with different curvatures and properties (a sphere, a pavilion of Félix Candela and the Trans World Flight of the New York John F. Kennedy Airport) (Figure 11).

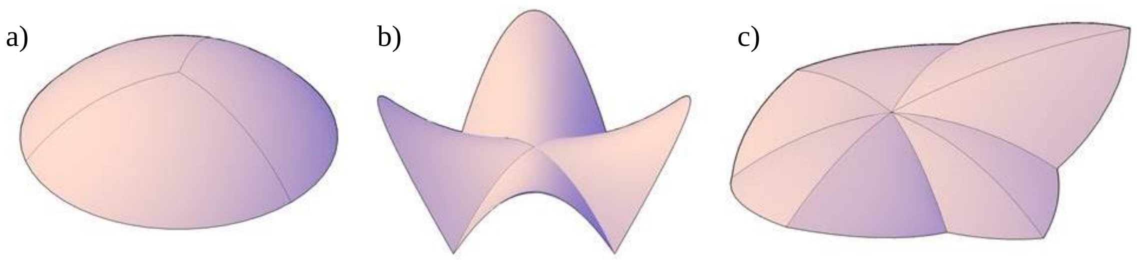

Fig. 11. a) Sphere b) Pavilion of Félix Candela c) Trans World Flight of the John F. Kennedy Airport

The stages of this method are:

- Stage 1: Rigidity

A geometric simulation of the deformations in the flexible rods is only possible if the structure has 1 degree of freedom. To achieve that, some ribs that fix the deployment direction of the structure are required and a technical solution that can create this behaviour is the stiffness technique of pyramids [42] (Figure 12).

a) b) c)

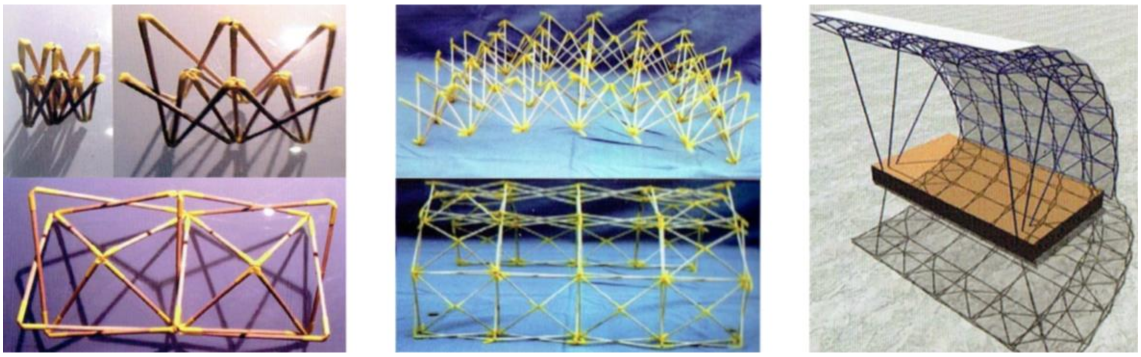

Fig. 12. a) Square modules with pyramids. These modules will only have one degree of freedom during deployment. b) Full cylinder with pyramids in the modules c) Half-cylinder with pyramids in the modules.

Some examples of the application of this technique can be observed in Figure 13.

a) b)

Fig. 13. a) Arch with pyramids b) Half-cylinder with pyramids.

Figure 14 is obtained if these ribs are applied to the 3 previous geometries.

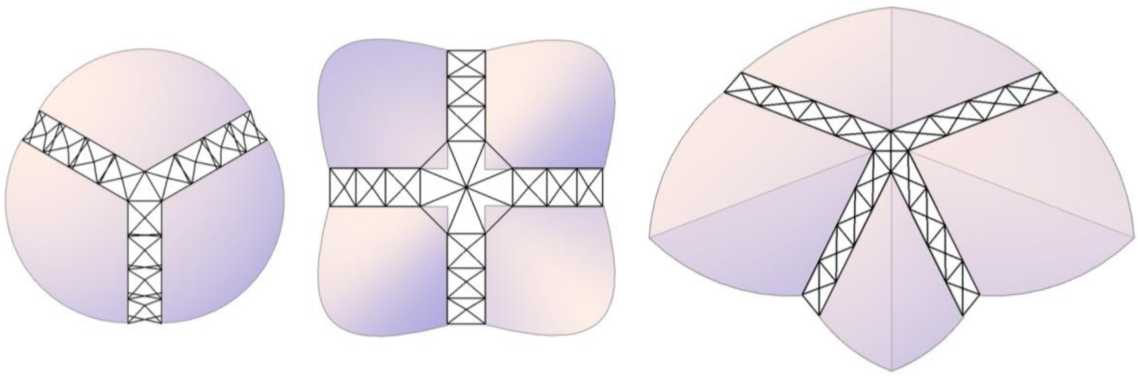

Fig. 14. Rigidity stage in the 3 previous geometries.

- Stage 2: Bistability

The next stage is to design a triangular tessellation in the spaces between the ribs. This triangular tessellation must be as bigger as possible in order to provide a prominent stability to the structure (Figure 15).

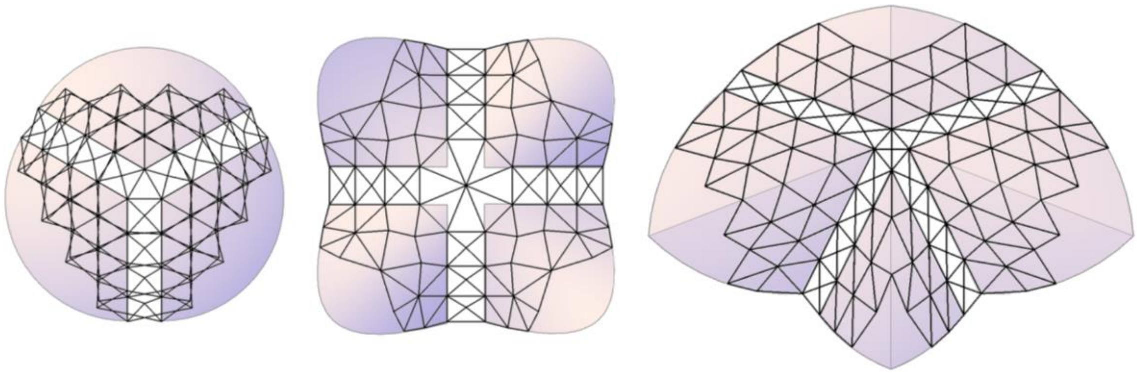

Fig. 15. Triangular tessellation of the bistability stage.

Then, principle 2 is applied to obtain the maximum stresses of compression (Figure 16)

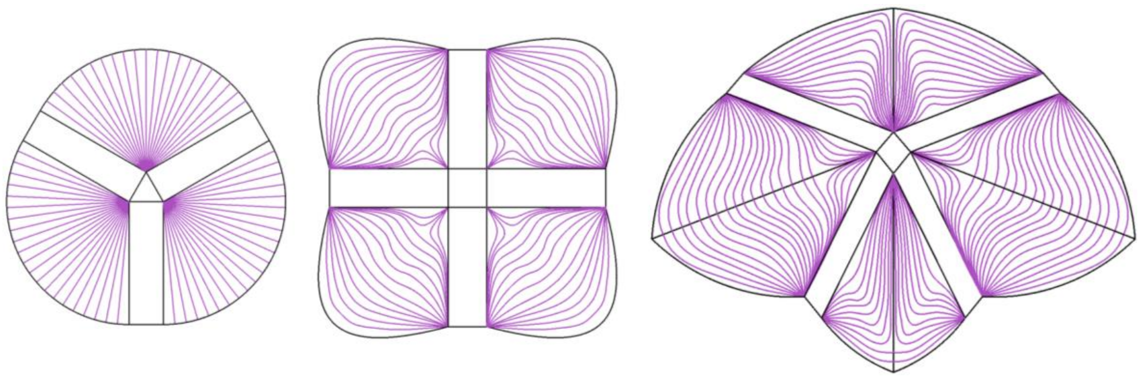

Fig. 16. Curves of the maximum stress of compression for the three study cases.

Finally, Figure 15 is compared with Figure 16 to know which **stiff** scissors are going to be converted to flexible scissors (red rods in Figure 17). These scissors will work only with compression during the deployment process and the **stiff** scissors will have a low deformation due to the geometric incompatibilities.

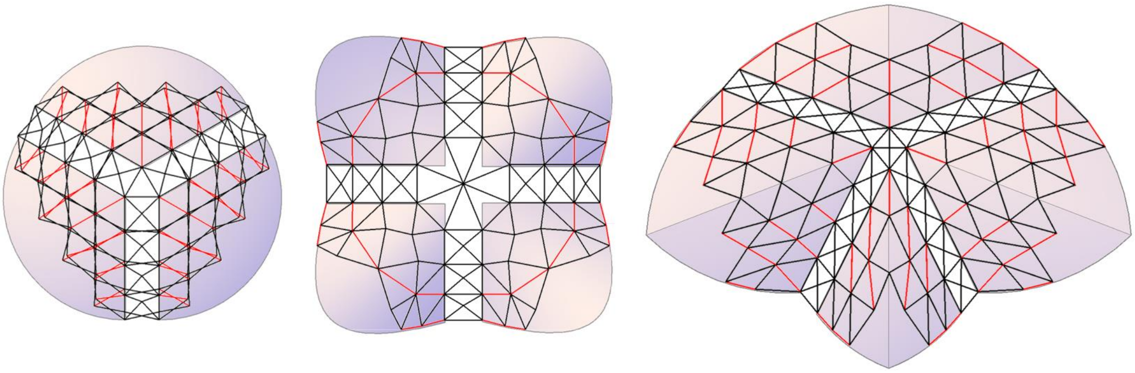

Fig. 17. Conversion of **stiff** scissors (black) to flexible scissors (red).

- Stage 3: Cover

The area of the previous structure that could not have a triangular tessellation will be designed with a 4-sided polygons tessellation (Figure 18).

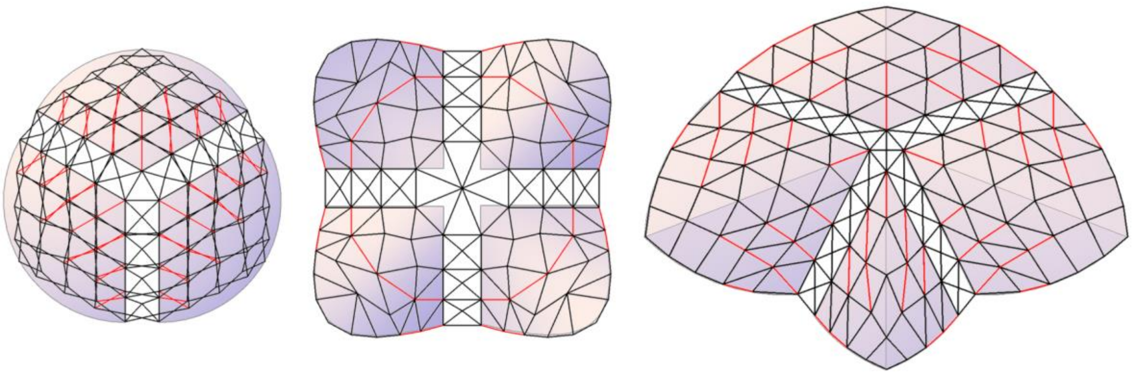

Fig. 18. 4-sided polygons tessellation in the rest of the surface.

The final structures are represented in Figure 19.

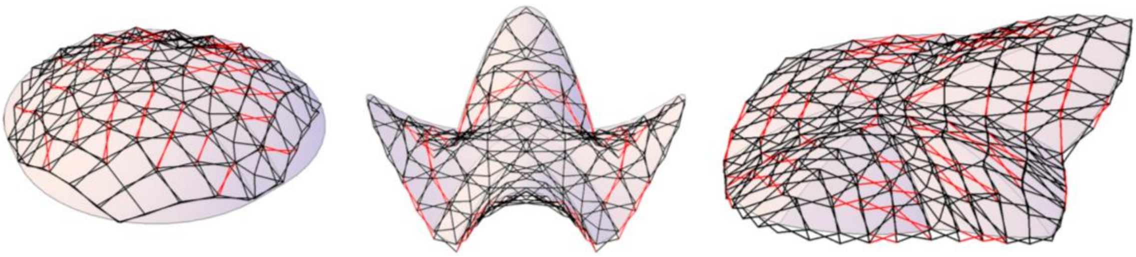

Fig. 19. Three-dimensional perspective after applying the RiBiCo method.

2.2.3. Built model

To compare the theoretical simulations with a real structure, a model of Figure 11 b) has been built using the same materials and joints from Figure 7 (Figure 20). In addition, the width for the rods of DM and ABS is 10mm.

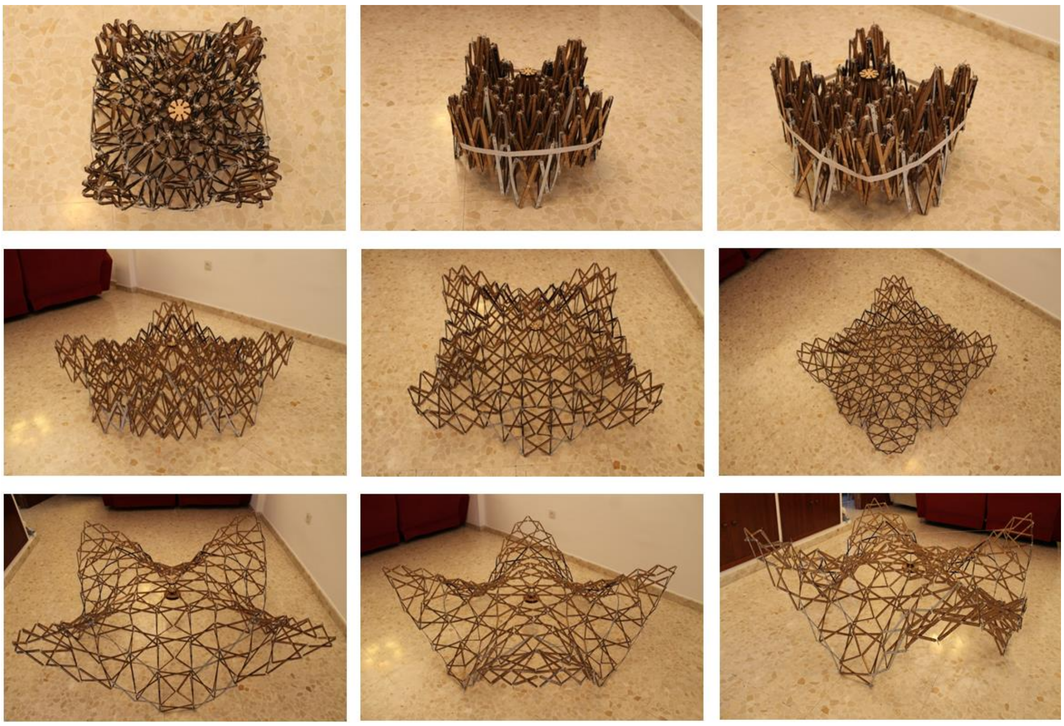

Fig. 20. Bistable Félix Candela pavilion with stiff and flexible rods using the RíBiCo method. The size of the folded position is 40 cm x 40 cm and the size of the unfolded position is 2 m x 2 m.

2.2.4. Results

After the model has been built, the comparison considering the geometric simulation and the FEM simulation can be done (Figure 21).

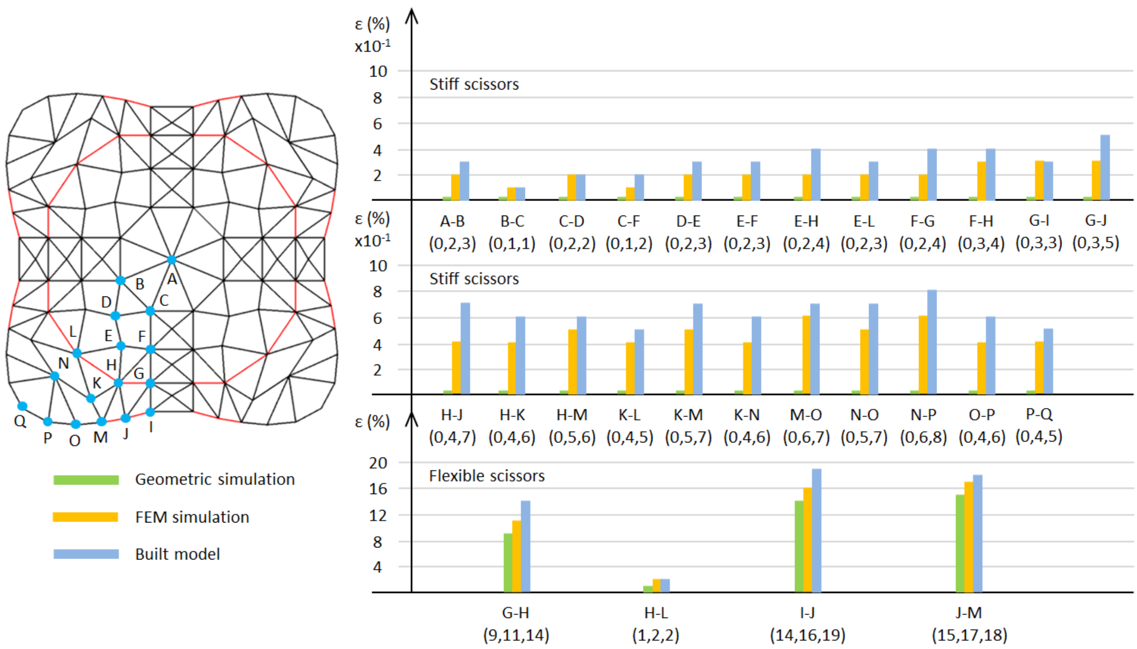

Fig. 21. Comparison of the highest deformations in the scissors.

As in the first method developed in this research, the source of errors comes from the simplification of the joints construction in the FEM simulation and the no consideration of the weight of the elements in the geometric simulation.

2.2.5. Dimension of the rods (the middle joint will be in the centre of each rod)

Stiff rods (units in cm)						
	A-B	B-C	C-D	C-F	D-E	E-F
Rod 1	12.76420	9.76929	7.95703	10.93438	7.22441	6.88477
Rod 2	12.76420	9.76929	8.93340	8.60420	6.70537	9.67147
	E-H	E-L	F-G	F-H	G-I	G-J
Rod 1	10.03765	10.03088	11.49792	10.13890	11.80646	9.75915
Rod 2	8.19510	11.65061	8.04066	11.08391	7.73212	10.20062
	H-J	H-K	H-M	K-L	K-M	K-N
Rod 1	12.80396	7.74518	9.64338	11.19507	9.02686	11.93300
Rod 2	8.84377	10.84178	9.88448	10.83005	6.16941	9.59637
	M-O	N-O	N-P	O-P	P-Q	-
Rod 1	7.21846	11.77186	10.30804	7.67707	6.47940	-
Rod 2	11.20594	12.97647	13.09869	11.67360	8.48936	-

Flexible rods (units in cm)				
	G-H	H-L	I-J	J-M
Rod 1	8.41057	14.90399	7.71254	7.03095
Rod 2	12.81282	11.44237	12.23184	11.23290

Table 2. Length of all rods (Félix Candela pavilion).

3. Joints

3.1. Joints that do not allow the geometric simulation

As has been established previously, the geometric simulation can only be done if the deployment process has 1 degree of freedom. However, an appropriate geometric simulation does not work if the joints have not the same behaviour. Different joints are currently available and not all can be used in the 2 methods proposed in this research. The joints that are not valid will be those that have a behaviour of a 4-rod mechanism (Figure 22).

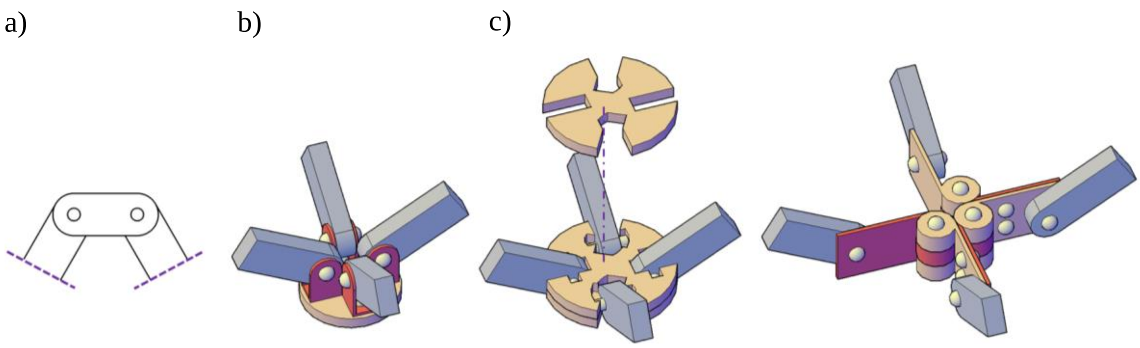

Fig. 22. a) 4 rods mechanism b) Joint designed by Félix Escrig-Pallarés and Jose Sánchez-Sánchez c) Joints designed by Kelvin Roovers and Niels de Temmerman.

3.2. Joints that allow the geometric simulation

On the other hand, the joints that allow a geometric simulation will be those that have just one perpendicular rotation to its plane (Figure 23). **However, it is important to highlight that these joints have a higher eccentricity in comparison with the joints of Fig. 21 and they are also prone to torsional instability**

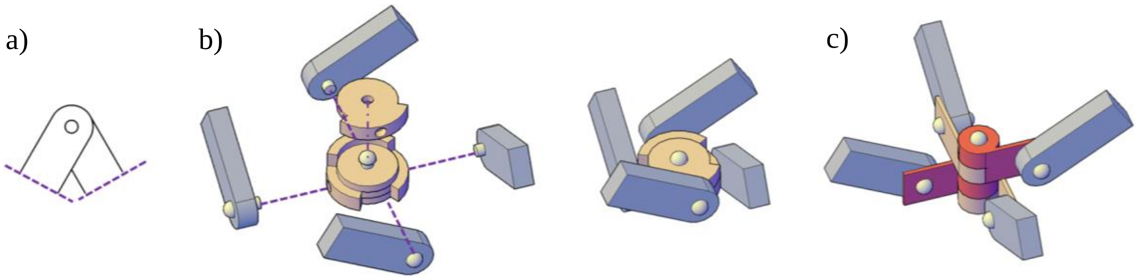

Fig. 23. a) Correct behaviour of a joint b) Joint designed by Carlos José García-Mora c) General joint.

4. Design and calculation of a real-scale bistable pavilion using stiff and flexible rods

The goal of this chapter is to apply the previous research to a real case where European regulation of structures will establish the conditions of fulfilment.

4.1. Design step

- Design geometry: Pavilion of Felix Candela with the shape and dimensions represented in Figure 24.

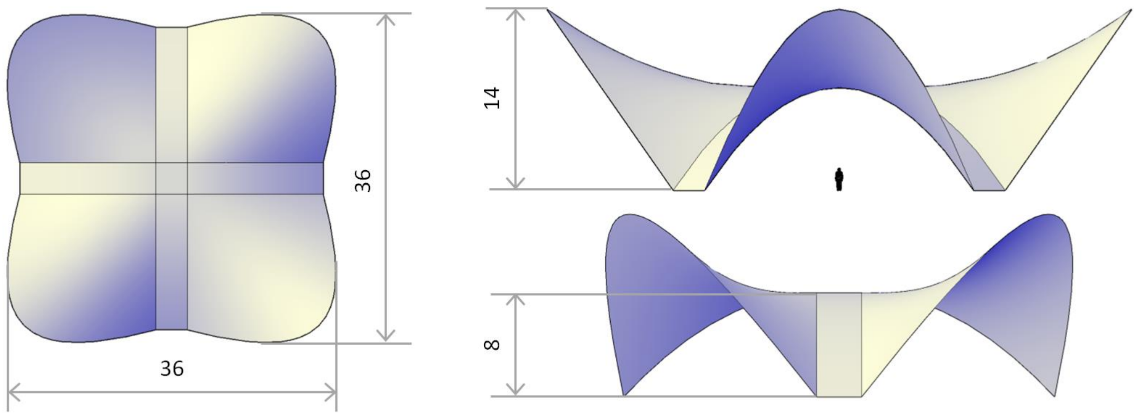

Fig. 24. Views of the geometry of the project (units in meters).

- Deployable structure: The RiBiCo method gives the geometry of Figure 25.

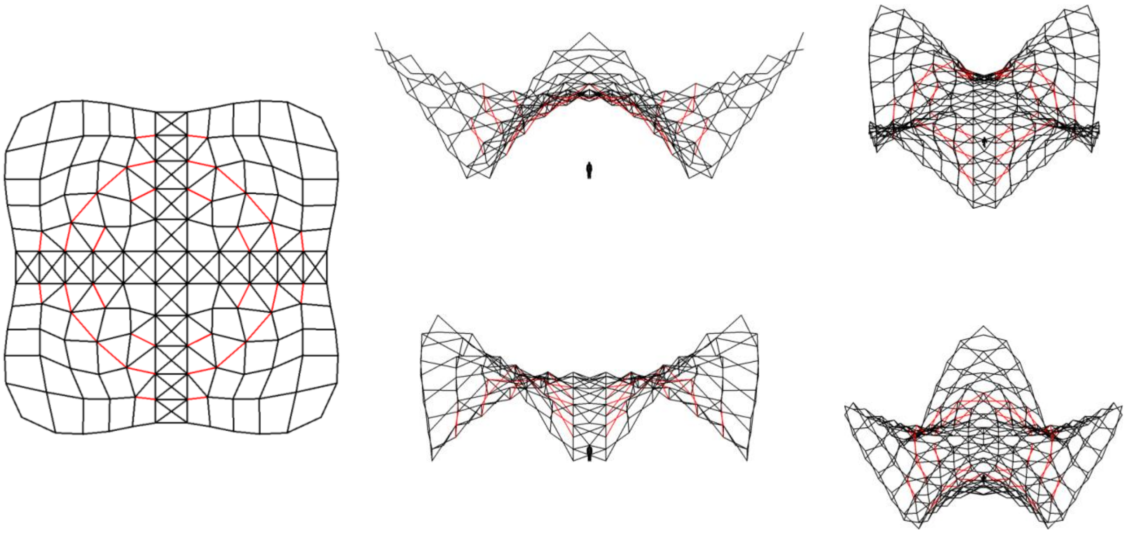

Fig. 25. Structure obtained after the use of the convergence surface method and the RiBiCo method. Black rods = stiff rods and red rod = flexible rods.

4.2. Material properties

The properties of the materials used in the calculation are shown in Table 3.

Material	Weight per unit volume (kN/m^3)	Coefficient of thermal expansion (°C^{-1})	Coefficient of Poisson	Modulus of elasticity (kN/m^2)
Aluminium	26.6018	2.358×10^{-5}	0.33	69637055
Cable	76.9729	1.320×10^{-5}	0	1.965×10^{8}
HDPE	90.4309	2×10^{-4}	0.46	1000000
Textile	120.27	1.170×10^{-5}	0.3	1

Table 3. Properties of the materials used in the calculation

It is important to highlight that the modulus of elasticity of the textile has been supposed as 1. The reason is to avoid the influence of the textile in the reduction of the deformations and to develop a calculation with a higher security coefficient.

4.3. Cross-section properties

The properties of the cross-sections used in the calculation are shown in Table 4.

Element	Type	Outside diameter (cm)	Wall thickness (cm)	Length 1 (cm)	Length 2 (cm)
Stiff rod	Hollow-circular	16	1	-	-
Flexible rod	Rectangular	-	-	16	2
Triangulation Rod	Hollow-circular	10	1	-	-
Cable	Solid-circular	2.5	-	-	-
Textile	Shell	-	-	5.30×10^{-6}	-

Table 4. Properties of the cross-sections used in the calculation

4.4. Joints properties

In order to have an important margin of security, the joints between all rods have been simulated as spherical joints (3 axes of rotation in the space, 3 directions of displacement in the space and no transmission of moment). Likewise, the connections between the structure and the ground are simulated using articulated joints (3 axes of rotation in the space, no displacement in the space and no transmission of moment).

4.5. Load properties

The next step is to define the properties of the loads during the calculation process (Table 5) (location: Seville, Spain).

Load	Value	
Own weight	-	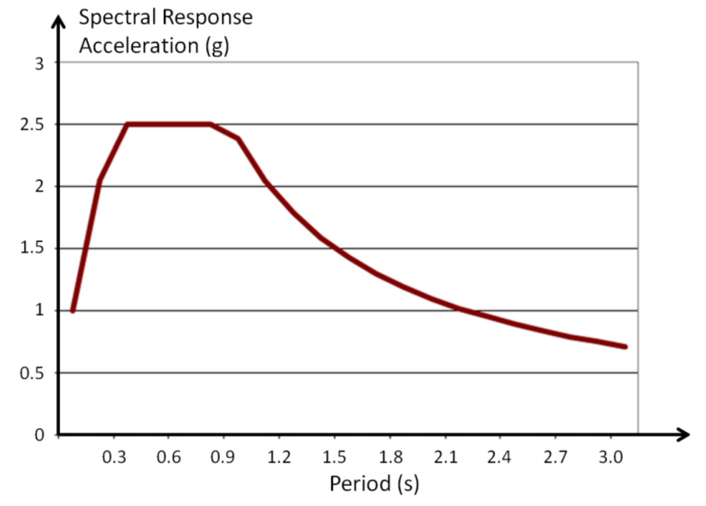
Illumination	**0.057 kN**	
Overload	1 kN/m^2	
Snow	1 kN/m^2	
Wind 0°	1 kN/m^2	
Wind 45°	1 kN/m^2	
Earthquake (U1)	**Figure on the right**	
Earthquake (U2)	**Figure on the right**	
Earthquake (U3)	**Figure on the right**	

Table 5. Properties of the loads used in the calculation

4.6. Combinations

The European regulation classifies load combinations (Table 6) in function of:

- Group 1: The goal of these combinations is to study the deformations and displacements of the structure. The name of these combinations is “Service Limit States” or SLS.

- Group 2: The goal of these combinations is to study the level of use of the material in structural elements. The name of these combinations is “Ultimate Limit States” or ULS.

Consequently, the general equation for any combination is:

$$\text{Combination} = K_1 \cdot Dead + K_2 \cdot Illumination + K_3 \cdot Snow + K_4 \cdot Overload + K_5 \cdot Wind\ 0^o + K_6 \cdot Wind\ 45^o + K_7 \cdot Earthquake \quad (1)$$

	Combination	K_1	K_2	K_3	K_4	K_5	K_6	K_7
SLS	SLS1 (snow with wind 0°)	1	1	1	0	0.6	0	0
	SLS2 (snow with wind 45°)	1	1	1	0	0	0.6	0
	SLS3 (wind 0°)	1	1	0.7	0	1	0	0
	SLS4 (wind 45°)	1	1	0.7	0	0	1	0
	SLS5 (overload with wind 0°)	1	1	0.7	1	0.6	0	0
	SLS6 (overload with wind 45°)	1	1	0.7	1	0	0.6	0
	SLS7 (earthquake)	1	1	0	0	0	0	1
ULS	ULS1 (snow with wind 0°)	1.35	1.35	1.50	0	0.90	0	0
	ULS2 (snow with wind 45°)	1.35	1.35	1.50	0	0	0.90	0
	ULS3 (wind 0°)	1.35	1.35	1.05	0	1.50	0	0
	ULS4 (wind 45°)	1.35	1.35	1.05	0	0	1.50	0
	ULS5 (overload with wind 0°)	1.35	1.35	1.05	1.50	0.90	0	0
	ULS6 (overload with wind 45°)	1.35	1.35	1.05	1.50	0	0.90	0

Table 6. K_i values for each combination

4.7. Additional elements to increase the stiffness of the structure in the final position of deployment

Deployable structures are very sensible in terms of vertical and horizontal deformations due to the use of articulated joints. This situation can be observed in the following picture where the vertical deformations against SLS5 are represented (Figure 26).

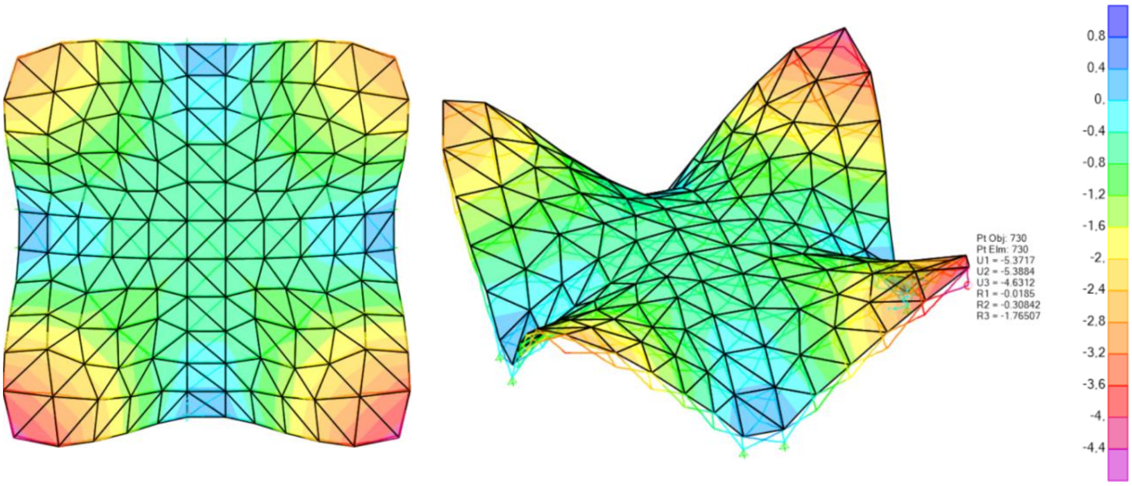

Fig. 26. Vertical deformations of the deployable structure if ELS5 is considered (units in meters).

To solve this situation and to obtain deformations that can fulfil the regulation, a set of cables and/or additional rods must be placed (cables will be used in this research). The first step is to obtain the distribution of the tractions (positive value) and compressions (negative value) on the superior side and on the inferior side of the surface (Figure 27).

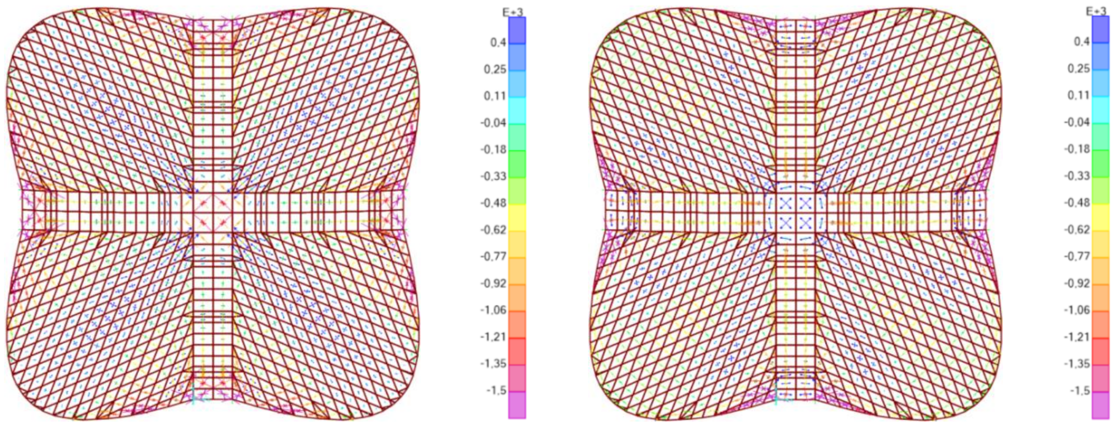

Fig. 27. (left side) Isostatic lines on the superior side of the surface; (right side) Isostatic lines on the inferior side of the surface.

The second step is to convert these arrays to spatial polylines using the software Karamba 3D and Python (left side of Figure 28). After that, a comparison between this result and the Figure 27 will be done in order to classify the stresses of the isostatic curves in function of the superior and inferior side of the surface. The result can be observed in Figure 28.

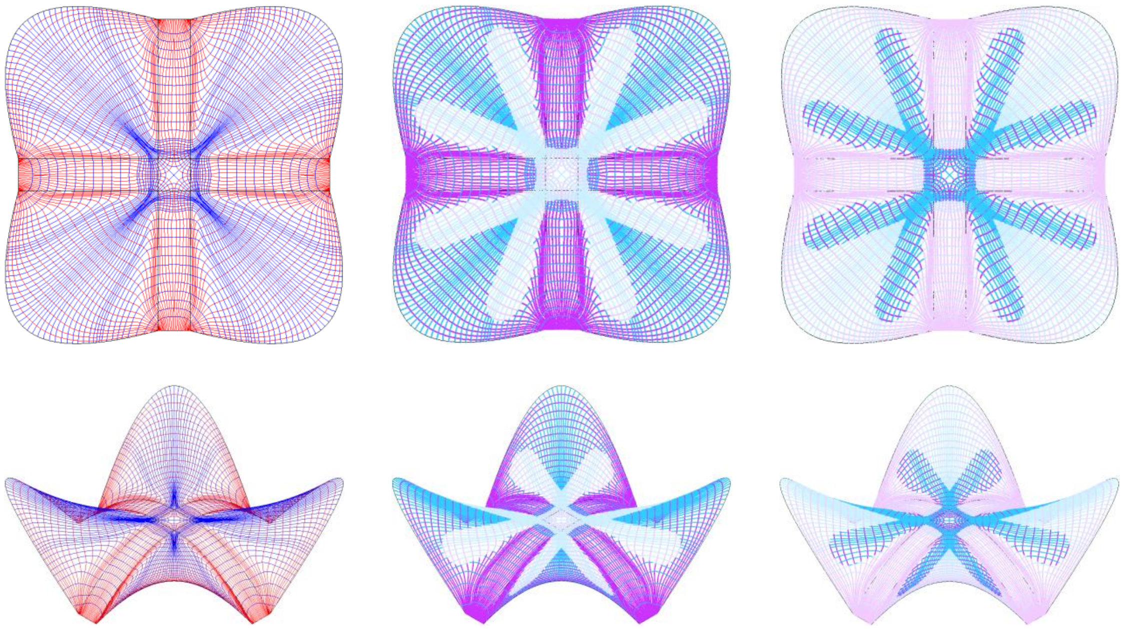

Fig. 28. (left side) Final isostatic curves; (central side) Classification of the isostatic curves in compression of traction on the superior side of the surface; (right side) Classification of the isostatic curves in compression of traction on the inferior side of the surface.

Where:

- Dark blue: Compression in isostatic curve with longitudinal direction.

- Light blue: Traction in isostatic curve with longitudinal direction.

- Dark purple: Compression in isostatic curve with transversal direction.

- Light purple: Traction in isostatic curve with transversal direction.

Once the isostatic curves have been obtained, the cables are placed following the direction of the isostatic curves of traction. The main goal of this strategy is to achieve a better structural behaviour in the cables reducing the price and the quantity of these elements.

4.8. Fulfilment of vertical deformations

After the position of the cables has been chosen, the maximum vertical deformations are shown in Figure 29 and the limit of vertical deformation is represented in Equation 2. In this case, the coefficient in function of the structure has a value of 300.

$$\frac{2 \cdot Distance\ between\ points\ considered}{Coefficient\ in\ function\ of\ the\ structure} \geq Maximum\ relative\ deformation \qquad (2)$$

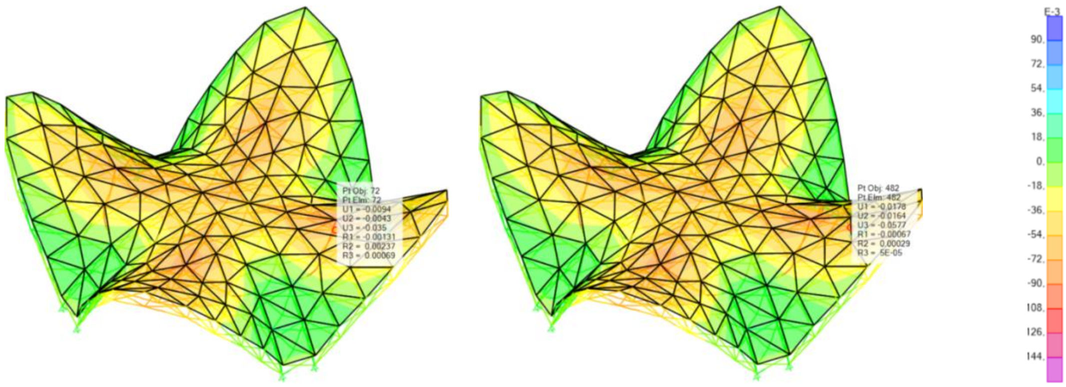

Fig. 29. Location of the maximum relative deformation if ELS5 is considered (units in meters).

Using the results of Figure 29:

$$\frac{2 \cdot 4.23}{300} \geq 5.77 - 3.5 \rightarrow 2.82\ cm \geq 2.27\ \mathrm{cm} \qquad (3)$$

4.9. Fulfilment of horizontal deformations

The behaviour of the structure against horizontal deformations (earthquake) and including the cables is represented in Figure 30.

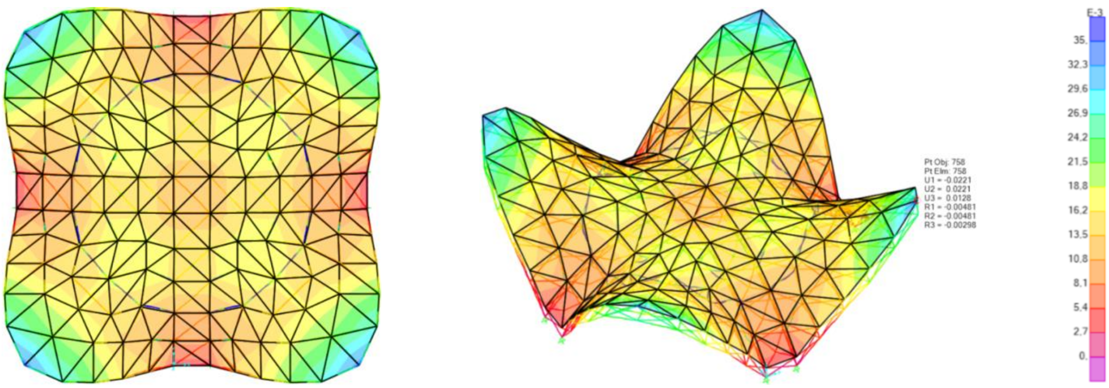

Fig. 30. Location of maximum horizontal displacement (units in meters).

The equation that verifies the fulfilment of horizontal deformations is the following (coefficient in function of the structure has a value of 250):

$$\frac{Height\ of\ the\ structure}{Coefficient\ in\ function\ of\ the\ structure} \geq 2 \cdot dtmax \rightarrow \frac{15.5}{250} \geq 2 \cdot \sqrt{U_1^2 + U_2^2} \qquad (4)$$

Using the Figure 30: $U_1 = U_2 = 0.022$ m.

$$\frac{15.5}{250} \geq 2 \cdot \sqrt{0.022^2 + 0.022^2} \rightarrow 6.2\ cm \geq 6.2\ cm \qquad (5)$$

4.10. Level of use of the structure

This calculation has been developed considering all ULS in the case with cables. The utilization ratios using the stress values are represented in Figure 31.

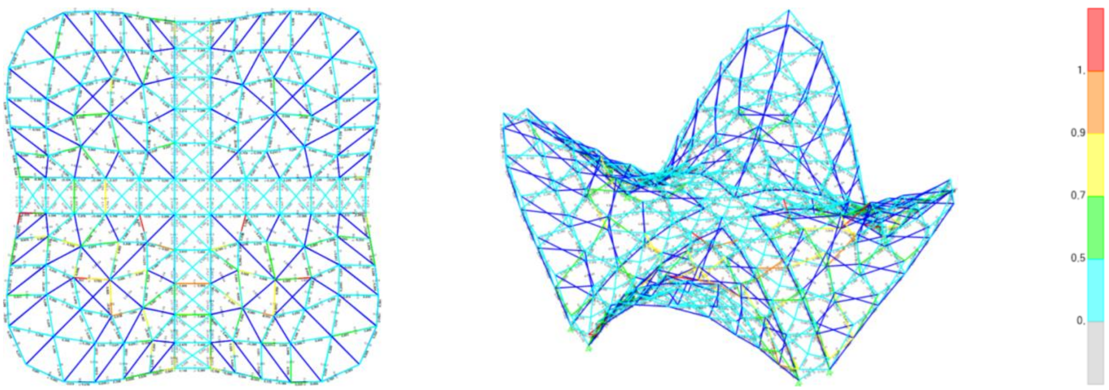

Fig. 31. Level of use of the structure.

As can be observed in the previous picture, there is not any rod with red colour and, in consequence, the level of use of all rods is below 100%. Otherwise, it would have been necessary to redesign the structure.

4.11. Natural frequencies

The last analysis that is going to be developed in this research is the study of the stiffness of the structure with cables. When this parameter is evaluated, M_1, M_2 and M_3 are always the most important vibration modes. In this case, the values of these vibration modes are around 1 Hz which means a prominent stiffness of the structure due to the incorporation of the cables. The result is represented in Figure 32.

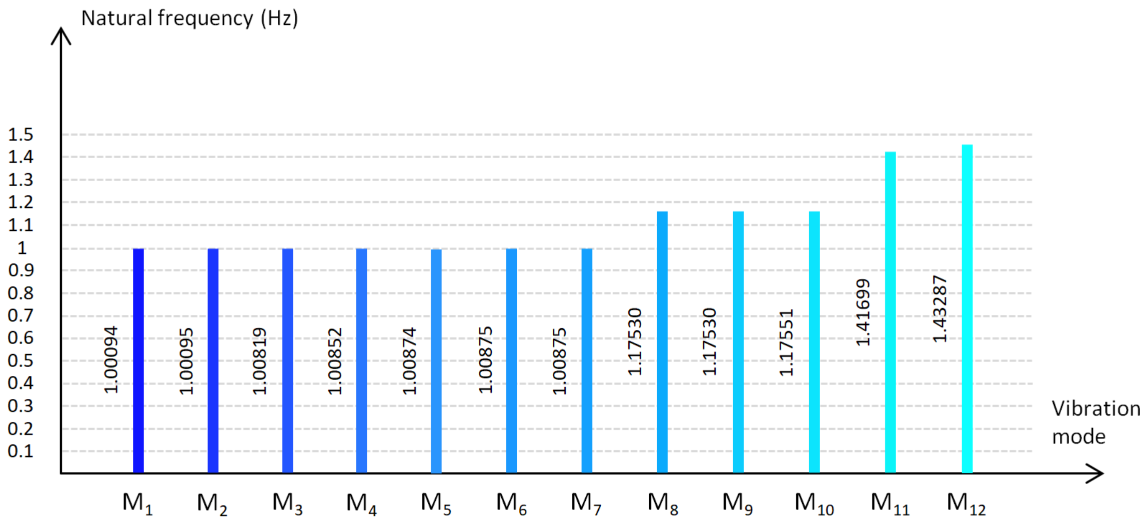

Fig. 32. Natural frequencies of the structure.

5. Conclusions

Two novel methods have been developed in this research for the design of bistable deployable structures with **stiff** and flexible rods. Having as reference the results of this paper, these methods have the following advantages and disadvantages in comparison with the traditional strategies to design this type of structures (simulation of the deployment using external loads):

a) Advantages:

a1) Generalization: The traditional methods work correctly for simple geometries such as cylinders or spheres. However, this analysis can take more time and effort in more complex shapes because it depends on how the external loads are applied. The methods developed in this research give valid results regardless of geometry.

a2) Geometric simulation: The methods proposed can approximate the deformations in the flexible rods during the deployment due to the geometric incompatibilities. Although this simulation introduces considerable errors because it does not consider not only elastic parameters but also the weight of the elements, it can give a rough idea about the distribution of the deformations in the flexible rods.

a3) Optimization: The classification of **stiff** and flexible rods in the traditional methods is achieved by analysing the stresses in the rods during the deployment after the application of external loads. However, some of these stresses can be reversed during the deployment causing a no stress of compression in the flexible rods. The methods of this research guarantee that the flexible rods will work only with compression during the whole deployment.

b) Disadvantages:

b1) Level of error in the results: The methods developed in this research cannot compete with the numerical accuracy in terms of value of deformations and stresses in comparison with the traditional methods.

Consequently, the design strategies of this paper are focused on an optimal distribution of the flexible and **stiff** rods. The subsequent exact value of the deformations during the deployment shall be obtained using the traditional methods.

6. Acknowledgements and formatting of funding sources

Research funded by Performance Ideas y Aplicaciones SL (Performance Ideas and Applications SL)

7. References

[1] Yan Chen, Zhong You, Tibor Tarnai, Threefold-symmetric Bricard linkages for deployable structures, International Journal of Solids and Structures, Volume 42, 2005, pp. 2287–2301, https://doi.org/10.1016/j.ijsolstr.2004.09.014

[2] Jiten Patel, G.K. Ananthasuresh, A kinematic theory for radially foldable planar linkages, International Journal of Solids and Structures, Volume 44, 2007, pp. 6279–6298, https://doi.org/10.1016/j.ijsolstr.2007.02.023

[3] A.P.Thrall, C.P.Quaglia, Accordion shelters: A historical review of origami-like deployable shelters developed by the US military, Engineering Structures, Volume 59, 2014, pp. 686–692, https://doi.org/10.1016/j.engstruct.2013.11.009

[4] Yao Chen, Jiayi Yan, Jian Feng, Pooya Sareh, Particle Swarm Optimization-Based Metaheuristic Design Generation of Non-Trivial Flat-Foldable Origami Tessellations With Degree-4 Vertices, Journal of Mechanical Design, Volume 143, 2021, pp. 1–12, https://doi.org/10.1115/1.4047437

[5] F. Escrig, Modular, Ligero, Transformable: Un Paseo Por La Arquitectura Ligera Móvil (Modular, Lightweight, Transformable: A Walk Through Mobile Lightweight Architecture), Universidad De Sevilla, Sevilla, 2012, ISBN: 978-84-472-1427-3

[6] Félix Candela, Emilio Pérez Piñero, Santiago Calatrava, Félix Escrig, Juan Pérez Valcárcel, Arquitectura Transformable (Transformable Architecture), Seville Higher Technical School of Architecture, 1993, ISBN: 84-600-8583-X

[7] F. Escrig, J.P. Valcárcel, Geometry of expandable space structures, International Journal of Space Structures, Volume 8, 1993, pp. 71–84, https://doi.org/10.1177/0266351193008001-208

[8] C. Hoberman, 1991. Radial expansion/retraction truss structures. US Patent. Number: 5.024.031

[9] S. Krishnan, Y. Li, Geometric design of deployable spatial structures made of threedimensional angulated members, Journal of Architectural Engineering, Volume 26, 2020, pp. 20–29, https://doi.org/10.1061/(asce)ae.1943-5568.0000416

[10] E. Pérez Piñero: Spanish Patent. Number: 266.801, 283.201, 311.901

[11] E. Pérez Piñero: U.S. Patent. Number: 3.185.164.

[12] E. Pérez Piñero, Teatros Desmontables (Deployable Theaters), Informes de la Construcción, Volume 24, June 1971, pp. 34–42, https://doi.org/10.3989/ic.1971.v24.i231.3360

[13] Z. You and S. Pellegrino, Foldable bar structures, International Journal of Solids and Structures, Volume 34, 1997, pp. 1825–1847, https://doi.org/10.1016/S0020-7683(96)00125-4

[14] A.P. Thrall, C.P. Quaglia, Accordion shelters: A historical review of origami-like deployable shelters developed by the US military, Engineering Structures, Volume 59, 2014, pp. 686–692, https://doi.org/10.1016/j.engstruct.2013.11.009

[15] C.P. Quaglia, A.J. Dascanio, A.P. Thrall, Bascule shelters: A novel erection strategy for origami-inspired deployable structures, Engineering Structures, Volume 75, 2014, pp. 276–287, https://doi.org/10.1016/j.engstruct.2014.06.003

[16] H. Yasuda, J. Yang, Reentrant Origami-Based Metamaterials with Negative Poisson's Ratio and Bistability, Physical Review Letters, Volume 114, 2015, pp. 1–5, https://doi.org/10.1103/PhysRevLett.114.185502

[17] Ketao Zhang, Jian S. Dai, A Kirigami-Inspired 8R Linkage and Its Evolved Overconstrained 6R Linkages With the Rotational Symmetry of Order Two, Journal of

Mechanisms and Robotics, Volume 6, 2014, pp. 1–12, https://doi.org/10.1115/1.4026337

[18] A. Fomin, L. Dvornikov, M. Paramonov, A. Jahr, To the theory of mechanisms subfamilies, in: International Conference on Mechanical Engineering, Automation and Control Systems 2015 (MEACS2015), Volume 124, 2015, pp. 1–4, https://doi.org/10.1088/1757-899x/124/1/012055

[19] A. Fomin, L. Dvornikov, J. Paik, Calculation of general number of imposed constraints of kinematic chains, in: International Conference on Industrial Engineering, Volume 206, 2017, pp. 1309–1315, https://doi.org/10.1016/j.proeng.2017.10.636

[20] Charis J. Gantes, Jerome J. Connor, Robert D. Logcher, Yechiel Rosenfeld, Structural Analysis and Design of Deployable Structures, Computers & Structures, Volume 32, 1989, pp. 661–669, https://doi.org/10.1016/0045-7949(89)90354-4

[21] J. Gantes Charis, Deployable Structures: Analysis and Design, WIT Press, 2001, ISBN: 1-85312-660-8

[22] C.Gantes, J.J.Connor, R.D.Logcher, Combining numerical analysis and engineering judgment to design deployable structures, Computers & Structures, Volume 40, 1991, pp. 431–440, https://doi.org/10.1016/0045-7949(91)90368-v

[23] C.J. Gantes, E. Konitopoulou, Geometric design of arbitrarily curved bi-stable deployable arches with discrete joint size, International Journal of Solids and Structures, Volume 41, 2014, pp. 5517–5540, https://doi.org/10.1016/j.ijsolstr.2004.04.030

[24] Yao Chen, Linzi Fan, Jian Feng, Kinematic of symmetric deployable scissor-hinge structures with integral mechanism mode, Computers & Structures, Volume 191, 2017, pp. 140–152, https://doi.org/10.1016/j.compstruc.2017.06.006

[25] L. Alegria Mira, R. Filomeno Coelho, A. P. Thrall, N. De Temmerman, Parametric evaluation of deployable scissor arches, Engineering Structures, Volume 99, 2015, pp. 479–491, https://doi.org/10.1016/j.engstruct.2015.05.013

[26] Uri Kirsch, Synthesis of structural geometry using approximation concepts, Computers & Structures, Volume 15, 1982, pp. 305–314, https://doi.org/10.1016/0045-7949(82)90021-9

[27] L. I. W. Arnouts, T. J. Massart, N. De Temmerman, P. Z. Berke, Multi-objective optimisation of deployable bistable scissor structures, Automation in Construction, Volume 114, 2020, pp. 1–14, https://doi.org/10.1016/j.autcon.2020.103154

[28] L. I. W. Arnouts, T. J. Massart, N. De Temmerman, P. Z. Berke, Computational modelling of the transformation of bistable scissor structures with geometrical imperfections, Engineering Structures, Volume 117, 2018, pp. 409–420, https://doi.org/10.1016/j.engstruct.2018.08.108

[29] A. Kaveh, Saeed Shojaee, Optimal Design of Scissor-Link Foldable Structures Using Ant Colony Optimization Algorithm, Computer-Aided Civil and Infrastructure Engineering, Volume 22, 2006, pp. 56–64, https://doi.org/10.1111/j.1467-8667.2006.00470.x

[30] Carlos J. García-Mora, Jose Sánchez-Sánchez, Geometric method to design bistable and non - bistable deployable structures of straight scissors based on the convergence surface, Mechanism and Machine Theory, Volume 146, 2020, pp. 1–31, https://doi.org/10.1016/j.mechmachtheory.2019.103720

[31] Carlos J. García-Mora, Jose Sánchez-Sánchez, The convergence surface method for the design of deployable scissor structures, Automation in Construction, Volume 122, 2021, pp. 1–19, https://doi.org/10.1016/j.autcon.2020.103488

[32] Carlos José García-Mora, Jose Sánchez-Sánchez, Limitations in the design of deployable structures with straight scissors using identical elements, International Journal of Solids and Structures, Volume 230–231, 2021, pp. 1–17, https://doi.org/10.1016/j.ijsolstr.2021.111171

[33] Paul Breiding, Bernd Sturmfels, Sascha Timme, 3264 Conics in a Second. Notices of the American Mathematical Society, Volume 67, 2020, pp. 30–37, https://doi.org/10.1090/noti2010

[34] Arseniy V. Akopyan, Alexander I. Bobenko, Incircular nets and confocal conics, Transactions of the American Mathematical Society, Volume 370, 2017, pp. 2825–2854, https://doi.org/10.1090/tran/7292

[35] Kelvin Roovers, Niels De Temmerman, Deployable scissor grids consisting of translational units, International Journal of Solids and Structures, Volume 121, 2017, pp. 45–61, https://doi.org/10.1016/j.ijsolstr.2017.05.015

[36] Kelvin Roovers, Niels De Temmerman, Geometric Design of Deployable Scissor Grids Consisting of Generalized Polar Units, Journal of the International Association for Shell and Spatial Structures, Volume 58, 2017, pp. 227–238, https://doi.org/10.20898/j.iass.2017.193.865

[37] Medium Density Fiberboard (MDF) properties, https://www.makeitfrom.com/material-properties/Medium-Density-Fiberboard-MDF, last update: 2020-05-30

[38] Stefan Ganev, Guy Gendron, Alain Cloutier, Robert Beauregard, Mechanical Properties of MDF as a Function of Density and Moisture Content, Wood and fiber science: Society of Wood Science and Technology, Volume 37, 2007, pp. 314–326, Corpus ID: 55764745

[39] Abdullah Özkalayci, Ibrahim Bektaş, Bekir Cihad Bal, Ayşenur Kiliç Ak, Effect of moisture content and density on some technological properties of fibreboard, Turkish Journal of Forestry, Volume 22, 2021, pp. 128–134, https://doi.org/10.18182/tjf.834279

[40] Overview of materials for Acrylonitrile Butadiene Styrene (ABS), http://www.matweb.com/search/DataSheet.aspx?MatGUID=3a8afcddac864d4b8f58d40570d2e5aa&ckck=1, last update: 2021-04-16

[41] Suraj Kumar Vishwakarma, Pankaj Pandey, Nitin Kumar Gupta, Characterization of ABS Material: A Review, Journal of Research in Mechanical Engineering, Volume 3, 2017, pp. 13–16, ISSN (Online) : 2321-8185

[42] Félix Escrig, Jose Sánchez. Arco desplegable de grandes dimensiones (deployable arch of big size). Spanish Patent. Number: 200500858